Downloaded 10/25/18 to 192.159.106.200. Redistribution subject to SEG license or copyright; see Terms of Use at http://library.seg.org/

# Improving reflection FWI reflectivity using LSRTM in the curvelet domain

*Adriano Gomes*, Zhuocheng Yang, CGG*

**Summary**

We investigate the benefits of improving the quantitative estimation of reflectivity in reflection FWI (RFWI). This is an important step of the inversion process, since it not only affects the generation of the synthetic reflection data, but also the generation of the "rabbit ears" along the reflection wavepaths. In our approach, the quantitative estimation of reflectivity is performed using least-squares reverse time migration (LSRTM), where the Hessian matrix and its inverse are estimated in the curvelet domain. Using synthetic and field data sets, we show how this approach can improve the reflectivity model and, therefore, benefit the RFWI velocity update. Finally, we discuss some of the limitations of this approach and some of the challenges that are not addressed by it.

**Introduction**

Reflection FWI (RFWI), firstly introduced by Chavent et al. (1994) and Clément et al. (2001), and reintroduced in its current form by Xu et al. (2012), has recently regained traction as a promising technology to retrieve low-wavenumber updates of velocity models using reflection data. Despite being presented in different forms, reflection FWI typically assumes the model $m$ can be separated into a long-wavelength (or background) component $m_0$ and a short-wavelength (or perturbation) component $\delta m$, such that:

$$m = m_0 + \delta m. \quad (1)$$

The goal of RFWI is then to update the background model $m_0$ in order to minimize the difference between the observed and synthetic reflection data. In general, this is achieved by iterating over the following steps:

1. Estimate the short-wavelength part of the model, or "model perturbation" $\delta m$, using the current background model $m_0$.
2. Generate synthetic reflection data using $m_0$ and $\delta m$.
3. Measure a residual between the input and synthetic reflection data.
4. Back-propagate the residual into the current model to obtain the velocity update along the reflection wavepaths, the so-called rabbit ears.

The first step of this process, estimating $\delta m$, is of great importance, since it affects not only the generation of the synthetic reflection data but also the generation of the rabbit ears along the reflection wavepaths. A variety of methods have recently been proposed to utilize this short-wavelength component in RFWI, e.g., using $\delta m$ to update the density model (Gomes and Chazalnoel, 2017), the impedance model (Zhou et al., 2018), or adding (and later removing) the short-wavelength component directly into the velocity model (Irabor and Warner, 2016).

Alternatively, $\delta m$ can be introduced as a reflectivity model (Xu et al., 2012; Alkhalifah and Wu, 2016; Vigh et al., 2016), in which case demigration has to be used to model the synthetic reflection data. One of the advantages of this approach is that it facilitates separation between the high-wavenumber and low-wavenumber components of the FWI gradient. In this scenario, the first step effectively becomes a least-squares reverse time migration (LSRTM) problem, i.e.,

$$\delta m = (L^T L)^{-1} L^T d, \quad (2)$$

where $L$ represents the Born modeling operator, $L^T$ represents its adjoint, the migration operator, and $d$ represents the recorded data. Equation 2 can be solved iteratively using local optimization methods such as steepest-descent or conjugate gradient (Nemeth et al., 1999). However, in the RFWI context, due to the computational cost involved, the LSRTM in the first step is normally reduced to a simple RTM, i.e., $\delta m \approx L^T d$, with the Hessian matrix $(L^T L)^{-1}$ sometimes replaced with diagonal approximations (Chavent et al., 1994).

Ignoring the effect of the Hessian matrix in Equation 2 exposes the RFWI reflectivity $\delta m$ to limitations of the migration operator and the acquisition geometry, which consequently affects the amplitude of the synthetic data $L\delta m$, as well as the balance between the contribution from different rabbit ears. To address these issues, previous approaches rely on schemes such as data matching and automatic gain control, or using kinematic-based objective functions that naturally include amplitude normalization terms (Ma and Hale, 2013; Luo et al., 2016). However, these methods can be prone to overboosting weak noise and either arbitrarily address, e.g., by automatic gain control, or do not address the issues of $\delta m$ that will be later used to generate the rabbit ears.

We first investigate, using a synthetic data set, the effects of relying on RTM instead of LSRTM to calculate the RFWI reflectivity. In addition, a more efficient approach using single-iteration LSRTM, more specifically, using curvelet-domain Hessian filters (CHF) (Wang et al., 2016), is proposed and validated with field data results.

© 2018 SEG

10.1190/segam2018-2996291.1

Downloaded 10/25/18 to 192.159.106.200. Redistribution subject to SEG license or copyright; see Terms of Use at http://library.seg.org/

### Effect of LSRTM in RFWI

We first used the model shown in Figure 1 to illustrate the effect of performing LSRTM for the RFWI reflectivity calculation. It consisted of a velocity model (Figure 1a) based on the Chevron 2014 benchmark model (Metivier et al., 2016) and a density model (Figure 1b) formed by a series of parallel layers.

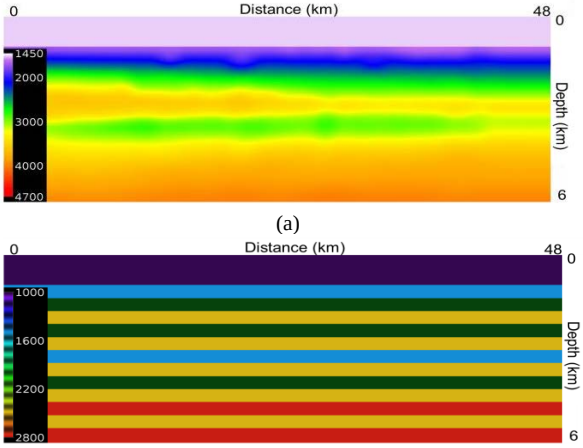


**Figure 1:** True models: (a) velocity model and (b) density model.

A ghost-free data set with maximum offset of 8 km was then generated using forward modeling. The initial model used for RFWI was the 1D model shown in Figure 2a. The velocity error correspondent to this model is shown in Figure 2b. The main challenge for RFWI in this case is to retrieve the low velocity zone below 3 km, which is beyond the diving wave penetration depth for the offsets available.

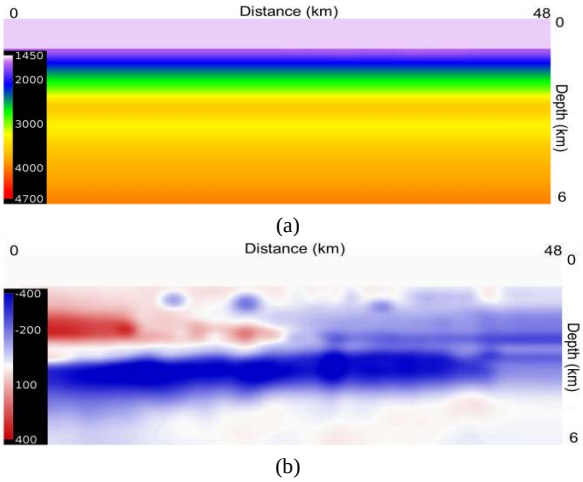


**Figure 2:** (a) Initial velocity model and (b) velocity error.

Next, we compared RFWI results using RTM and LSRTM to calculate the reflectivity model. In the RTM case, an amplitude match between synthetic data $L\delta m$ and input data $d$ was applied prior to the residual calculation to minimize the error produced by ignoring the Hessian matrix. In addition, a diagonal approximation of the Hessian was applied to compensate for source-side illumination. However, in the LSRTM case, those steps were not necessary since the LSRTM itself will compensate for the Hessian effects and produce more accurate amplitudes.

Figures 3a and 3b show the reflectivity models obtained in the first RFWI iteration, using RTM and LSRTM, respectively, as described above. The maximum frequency in this case was 3 Hz. Although the diagonal approximation applied to the RTM was able to produce relatively balanced amplitudes, it still did not fully compensate for the Hessian effects, as can be noted by comparing it to the LSRTM result (Figure 3b).

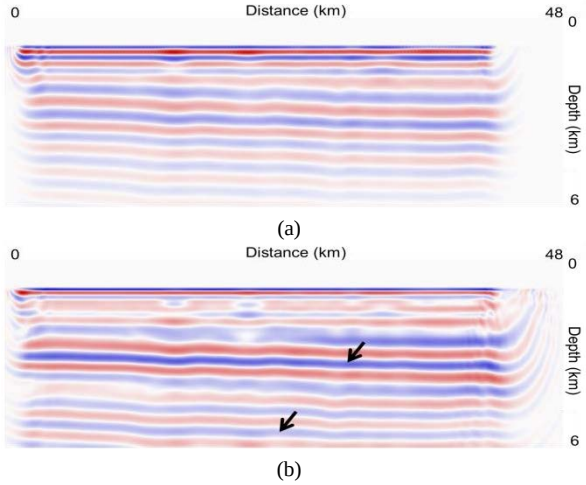


**Figure 3:** 3 Hz RFWI reflectivity model using: (a) compensated RTM and (b) LSRTM.

We then applied RFWI starting from the initial model shown in Figure 2a and a fixed constant density model. The transmitted wave data were muted prior to the inversion. A total of 35 RFWI iterations were performed from 3 Hz to 6 Hz, with each iteration requiring the recalculation of $\delta m$ using the current background model. Figures 4a and 4b show the RFWI result using RTM and LSRTM, respectively, to calculate the reflectivity model at each iteration. Compared to the true velocity error (Figure 2b), it is clear that the LSRTM-based RFWI result (Figure 4b) is able to invert the main features of the model, with the perturbation distribution resembling the true result. In contrast, the RTM-based RFWI (Figure 4a) suffers from

© 2018 SEG

10.1190/segam2018-2996291.1

Downloaded 10/25/18 to 192.159.106.200. Redistribution subject to SEG license or copyright; see Terms of Use at http://library.seg.org/

localized artifacts, as indicated by the arrows, resulting from the accumulated effects of neglecting the Hessian matrix.

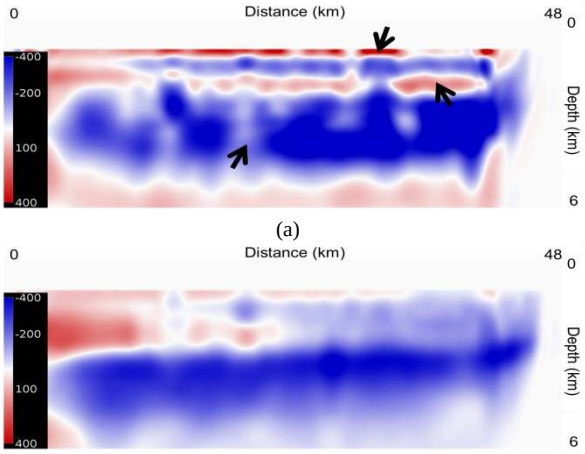


**Figure 4:** RFWI results starting from initial model shown in Figure 2a: (a) using RTM to calculate the reflectivity and (b) using LSRTM to calculate the reflectivity.

The results in Figure 4 show the benefits of using a more accurate method to calculate the RFWI reflectivity model. Nevertheless, the cost of using LSRTM at every iteration cannot be overlooked for large 3D data sets. Therefore, a more efficient compromise needs to be considered for realistic applications.

**Single-iteration LSRTM**

One way to improve the RFWI reflectivity model without dramatically increasing its cost is by using so-called single-iteration LSRTM methods, which aim to fully compensate for the Hessian effects while requiring at most two migrations. Many different ideas have been proposed to achieve this goal, e.g., the approximate inverse Born modeling operator (Hou and Symes, 2014), point-spread function deconvolution (Fletcher et al., 2016), and non-linear Hessian filters (Guitton, 2004).

Recently, Wang et al. (2016) proposed to compute the non-linear Hessian filters in the curvelet domain by minimizing the objective function $f$:

$$f(s) = \|C[L^T d] - sC[(L^T L)L^T d]\|^2 + \epsilon\|s\|^2, \qquad (3),$$

where $s$ represents the curvelet-domain Hessian filters (CHF), $C$ represents the curvelet transform, and $\epsilon$ is a weight factor for the normalization term. In the context of RFWI, the reflectivity can then be determined by:

$$\delta m \approx C^{-1}\big[|s|C[L^T d]\big], \qquad (4),$$

where $C^{-1}$ denotes the inverse curvelet transform. This approach has been shown to compensate for the Hessian effects while preventing the boosting of noise in poor signal-to-noise ratio (S/N) areas of the reflectivity, due to the sparseness introduced by the curvelet transform.

We propose to use Equation 4 to calculate the RFWI reflectivity instead of the more costly iterative LSRTM. In the next section, we show the results of this method applied to a field data example.

**Field data example**

The data used for this test are from a deep-water survey over the Perdido fold belt, in the Mexican side of the Gulf of Mexico (GoM). The seismic data were acquired using a flat-cable wide-azimuth (WAZ) acquisition configuration with maximum offset of 8.1 km along the cables and 4.2 km across the cables.

We first evaluated the impact of the improved reflectivity model in the synthetic reflection data generated during RFWI. Figures 5a, 5b, and 5c show, respectively, the 4 Hz reflectivity obtained with RTM, iterative LSRTM, and single-iteration LSRTM for the first RFWI iteration. Figures 5d, 5e, and 5f show the synthetic reflection data sets obtained by demigration using the respective reflectivity models. It is noticed that later arrivals have improved S/N in Figures 5e and 5f, as a result of the improved amplitudes of deep reflectors observed in Figures 5b and 5c. It is also observed that the single-iteration LSRTM was able to achieve a comparable result at a fraction of the iterative LSRTM cost.

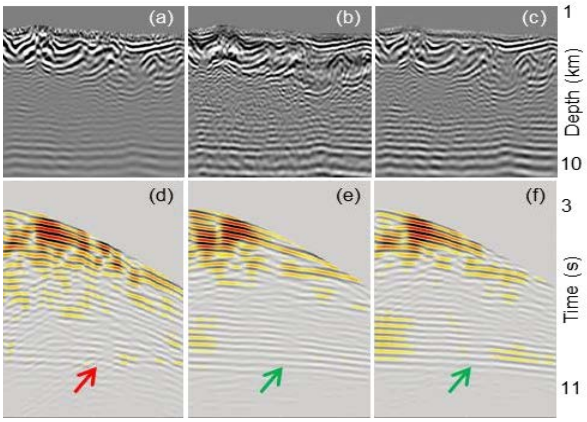


**Figure 5:** Reflectivity model obtained using: (a) RTM, (b) iterative LSRTM, and (c) single-iteration LSRTM (CHF); and synthetic reflection data: (d), (e), and (f) obtained by demigration using (a), (b), and (c), respectively.

© 2018 SEG

10.1190/segam2018-2996291.1

Downloaded 10/25/18 to 192.159.106.200. Redistribution subject to SEG license or copyright; see Terms of Use at http://library.seg.org/

We then performed 10 iterations of RFWI using a maximum frequency of 4 Hz. As reference, the migrated image using the initial model is presented in Figure 6a, which shows strong discontinuity of the deep events due to velocity errors in the overburden. Figure 6b shows the same section, but migrated with the final RFWI model using RTM to obtain the reflectivity. Although improvements can be observed in many locations, there are still some discontinuities in the Wilcox and Cretaceous formations, as indicated by the arrows. Finally, Figure 6c shows the image migrated with the RFWI model using single-iteration LSRTM for reflectivity. It is clear that the improved reflectivity model had a positive impact on the inverted velocities, resulting in more focused and continuous events.

## Discussion and limitations

Although compensating for the Hessian effects in the RFWI reflectivity model has clear benefits, there are still limitations that must be discussed.

First of all, the single-iteration LSRTM methods normally rely on a windowed matching process, assuming a smooth transition of the illumination problem, which is not always the case. One possible alternative is to use the matching filters to pre-condition the iterative LSRTM, as proposed by Wang et al. (2017), thus speeding up its convergence.

Another restriction concerns the least-squares migration in general, including iterative methods, which are limited by effects that are not taken into account, such as transmission loss, attenuation, and mode conversion.

Finally, having the correct amplitudes in the reflectivity model will not automatically prevent stronger events from contributing more in the RFWI inversion, since they still generate stronger reflection energy, which result in stronger rabbit ears. However, the single-iteration LSRTM reflectivity can be naturally combined with kinematic-based objective functions, which normalize the contribution from different events in the velocity update stage. These objective functions will also benefit from the improved reflectivity and synthetic data, as indicated by Figure 5.

## Conclusions

Based on synthetic and field data results, we show the importance of compensating for the Hessian matrix effect in RFWI, i.e., using LSRTM instead of RTM for the calculation of its reflectivity. However, the cost of doing so cannot be overlooked for large 3D data sets. Therefore, we propose a more efficient approach using single-iteration LSRTM, more specifically, using curvelet-domain Hessian filters. Despite some limitations, this approach was able to improve the RFWI results when compared to those using RTM to calculate the reflectivity. In addition, some of the discussed limitations can potentially be mitigated by using kinematic-based objective functions.

## Acknowledgments

We thank CGG Multi-Client & New Ventures and the Mexican Comisión Nacional de Hidrocarburos for permission to show these results. We also thank Ping Wang for fruitful discussions and Gilles Lambaré, Xie Yi and Shannon Basile for their suggestions.

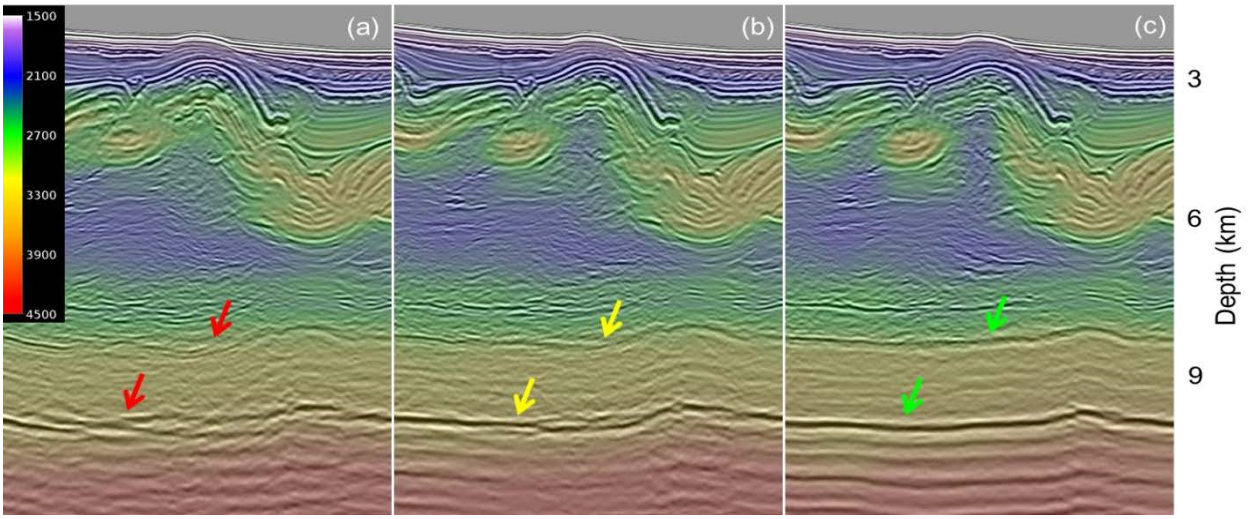


**Figure 6:** RTM migration using: (a) Initial velocity model, (b) RFWI model using RTM for reflectivity and (c) RFWI model using single-iteration LSRTM for the reflectivity. For both tests, 10 iterations of RFWI using a maximum frequency of 4 Hz were performed. The correspondent velocity models are shown in the background.

© 2018 SEG

10.1190/segam2018-2996291.1

## REFERENCES


Alkhalifah, T., and Z. Wu, 2016, The natural combination of full and image-based waveform inversion: Geophysical Prospecting, **64**, 19–30, https://doi.org/10.1111/1365-2478.12264.

Chavent, G., F. F. Clément, and S. Gómez, 1994, Automatic determination of velocities via migration-based traveltime waveform inversion: A synthetic data example: 64th Annual International Meeting, SEG, Expanded Abstracts, 1179–1182, https://doi.org/10.1190/1.1822731.

Clément, F., G. Chavent, and S. Gómez, 2001, Migration-based traveltime waveform inversion of 2-D simple structures: A synthetic example: Geophysics, **66**, 845–860, https://doi.org/10.1190/1.1444974.

Fletcher, R., D. Nichols, R. Bloor, and R. Coates, 2016, Least-squares migration - Data domain versus image domain using point spread functions: The Leading Edge, **35**, 157–162, https://doi.org/10.1190/tle35020157.1.

Gomes, A., and N. Chazalnoel, 2017, Extending the reach of full-waveform inversion with reflection data: Potential and challenges: 87th Annual International Meeting, SEG, Expanded Abstracts, 1454–1459, https://doi.org/10.1190/segam2017-17731403.1.

Guitton, A., 2004, Amplitude and kinematic corrections of migrated images for nonunitary imaging operators: Geophysics, **69**, 1017–1024, https://doi.org/10.1190/1.1778244.

Hou, J., and W. W. Symes, 2014, An approximate inverse to the extended born modeling operator: 84th Annual International Meeting, SEG, Expanded Abstracts, 3784–3789, https://doi.org/10.1190/segam2014-0769.1.

Irabor, K., and M. Warner, 2016, Reflection FWI: 86th Annual International Meeting, SEG, Expanded Abstracts, 1136–1140, https://doi.org/10.1190/segam2016-13944219.1.

Luo, Y., Y. Ma, Y. Wu, H. Liu, and L. Cao, 2016, Full-traveltime inversion: Geophysics, **81**, no. 5, R261–R274, https://doi.org/10.1190/geo2015-0353.1.

Ma, Y., and D. Hale, 2013, Wave-equation reflection traveltime inversion with dynamic warping and full-waveform inversion: Geophysics, **78**, no. 6, R223–R233, https://doi.org/10.1190/geo2013-0004.1.

Metivier, L., R. Brossier, E. Oudet, Q. Mérigot, and J. Virieux, 2016, An optimal transport distance for full-waveform inversion: Application to the 2014 Chevron benchmark data set: 86th Annual International Meeting, SEG, Expanded Abstracts, 1278–1283, https://doi.org/10.1190/segam2016-13870096.1.

Nemeth, T., C. Wu, and G. Schuster, 1999, Least-squares migration of incomplete reflection data: Geophysics, **64**, 208–221, https://doi.org/10.1190/1.1444517.

Vigh, D., K. Jiao, X. Cheng, D. Sun, and W. Lewis, 2016, Earth-model building from shallow to deep with full- waveform inversion: The Leading Edge, **35**, 1025–1030, https://doi.org/10.1190/tle35121025.1.

Wang, M., S. Huang, and P. Wang, 2017, Improved iterative least-squares migration using curvelet-domain Hessian filters: 87th Annual International Meeting, SEG, Expanded Abstracts, 4555–4560, https://doi.org/10.1190/segam2017-17783350.1.

Wang, P., A. Gomes, Z. Zhang, and M. Wang, 2016, Least-squares RTM: Reality and possibilities for subsalt imaging: 86th Annual International Meeting, SEG, Expanded Abstracts, 4204–4209, https://doi.org/10.1190/segam2016-13867926.1.

Xu, S., D. Wang, F. Chen, Y. Zhang, and G. Lambaré, 2012, Full waveform inversion for reflected seismic data: 74th Annual International Conference and Exhibition, EAGE, Extended Abstracts, W024, https://doi.org/10.3997/2214-4609.20148725.

Zhou, W., R. Brossier, S. Operto, J. Virieux, and P. Yang, 2018, Velocity model building by waveform inversion of early arrivals and reflections: A 2D case study with gas-cloud effects: Geophysics, **83**, no. 2, R141–R157, https://doi.org/10.1190/geo2017-0282.1.


Downloaded 10/25/18 to 192.159.106.200. Redistribution subject to SEG license or copyright; see Terms of Use at http://library.seg.org/